Published for SISSA by Springer

Received: *April 24, 2013*
Revised: *October 7, 2013*
Accepted: *November 16, 2013*
Published: *December 13, 2013*

Linearized stability analysis of gravastars in noncommutative geometry

Francisco S.N. Lobo[a] **and Remo Garattini**[b,c]

[a] *Centro de Astronomia e Astrofísica da Universidade de Lisboa, Campo Grande, Ed. C8, 1749-016 Lisboa, Portugal*
[b] *Facoltà di Ingegneria, Università degli Studi di Bergamo, Viale Marconi 5, 24044 Dalmine (Bergamo), Italy*
[c] *INFN — Sezione di Milano, Via Celoria 16, Milan, Italy*

E-mail: flobo@cii.fc.ul.pt, Remo.Garattini@unibg.it

Abstract: In this work, we find exact gravastar solutions in the context of noncommutative geometry, and explore their physical properties and characteristics. The energy density of these geometries is a smeared and particle-like gravitational source, where the mass is diffused throughout a region of linear dimension $\sqrt{\alpha}$ due to the intrinsic uncertainty encoded in the coordinate commutator. These solutions are then matched to an exterior Schwarzschild spacetime. We further explore the dynamical stability of the transition layer of these gravastars, for the specific case of $\beta = M^2/\alpha < 1.9$, where M is the black hole mass, to linearized spherically symmetric radial perturbations about static equilibrium solutions. It is found that large stability regions exist and, in particular, located sufficiently close to where the event horizon is expected to form.

Keywords: Non-Commutative Geometry, Classical Theories of Gravity, Black Holes

ArXiv ePrint: 1004.2520

doi:10.1007/JHEP12(2013)065

JHEP12(2013)065

Contents

JHEP12(2013)065

1 Introduction

About a decade ago, an alternative picture for the final state of gravitational collapse has emerged [1–4]. The latter, denoted as a gravastar (*grav*itational *va*cuum *star*), consists of an interior compact object matched to an exterior Schwarzschild vacuum spacetime, at or near where the event horizon is expected to form. Therefore, these alternative models do not possess a singularity at the origin and have no event horizon, as its rigid surface is located at a radius slightly greater than the Schwarzschild radius. More specifically, the gravastar picture, proposed by Mazur and Mottola [1–4], has an effective phase transition at/near where the event horizon is expected to form, and the interior is replaced by a de Sitter condensate. This new emerging picture consisting of a compact object resembling ordinary spacetime, in which the vacuum energy is much larger than the cosmological vacuum energy, is also denoted as a "dark energy star" [5, 6]. In fact, a wide variety of gravastar models have been considered in the literature [7–17] and their observational signatures have also been explored [18–25]. It was argued that the resulting gravitational condensate star configuration resolve all black hole paradoxes, and provides a testable alternative to black holes as the final state of complete gravitational collapse [26].

In this work, we consider a further extension of the gravastar picture in the context of noncommutative geometry. The dynamical stability of the transition layer of these gravastars to linearized spherically symmetric radial perturbations about static equilibrium solutions is also explored. The analysis of thin shells [27–34] and the respective linearized stability analysis of thin shells has been recently extensively considered in the literature, and we refer the reader to refs. [35–50] for details. Relative to the context of the stability analysis, the radial stability of the continuous pressure gravastar was studied using the conventional Chandrasekhar method, for radial pulsations and small perturbations around a stable equilibrium [51]. The study of the oscillation spectrum was also studied [52] in the context of dark energy stars, where the frequencies of the fundamental mode and the higher overtones are strongly affected by the dark energy content. It was also argued that this can be used in the future to detect the presence of dark energy in neutron stars and to constrain the dark-energy models.

In the context of noncommutative geometry, an interesting development of string/M-theory has been the necessity for spacetime quantization, where the spacetime coordinates become noncommuting operators on a D-brane [53, 54]. The noncommutativity of spacetime is encoded in the commutator $[\mathbf{x}^{\mu}, \mathbf{x}^{\nu}] = i\,\theta^{\mu\nu}$, where $\theta^{\mu\nu}$ is an antisymmetric matrix which determines the fundamental discretization of spacetime. It has also been shown that noncommutativity eliminates point-like structures in favor of smeared objects in flat spacetime [55]. Thus, one may consider the possibility that noncommutativity could cure the divergences that appear in general relativity. The effect of the smearing is mathematically implemented with a substitution of the Dirac-delta function by a Gaussian distribution of minimal length $\sqrt{\alpha}$. In particular, the energy density of a static and spherically symmetric, smeared and particle-like gravitational source has been considered in the following form [56]

$$\rho_{\alpha}(r) = \frac{M}{(4\pi\alpha)^{3/2}}\,\exp\left(-\frac{r^2}{4\alpha}\right), \tag{1.1}$$

where the mass M is diffused throughout a region of linear dimension $\sqrt{\alpha}$ due to the intrinsic uncertainty encoded in the coordinate commutator.

The Schwarzschild metric is modified when a non-commutative spacetime is taken into account [56, 57]. Although one may consider the analysis in a general static and spherically symmetric line element in the following form

$$ds^2 = -A(r)dt^2 + A^{-1}(r)dr^2 + R^2(r)(d\theta^2 + \sin^2\theta\, d\phi^2) \tag{1.2}$$

or in isotropic coordinates where the line element is given by by $ds^2 = -e^{2\varphi(r)}dt^2 + e^{\psi(r)}[dr^2 + r^2(d\theta^2 + \sin^2\theta\, d\phi^2]$, where the $\varphi(r)$ and $\psi(r)$ are finite everywhere, we emphasize that physically correct results do not depend on the coordinate system used. In this context, we use Schwarzschild coordinates throughout this work.

Thus, the solution obtained is described by the following spacetime metric

$$ds^2 = -f(r)\,dt^2 + \frac{dr^2}{f(r)} + r^2\,(d\theta^2 + \sin^2\theta\, d\phi^2)\,, \tag{1.3}$$

JHEP12(2013)065

with $f(r) = 1 - 2m(r)/r$, where the mass function is defined as

$$m(r) = \frac{2M}{\sqrt{\pi}}\gamma\left(\frac{3}{2}, \frac{r^2}{4\alpha}\right), \tag{1.4}$$

and

$$\gamma\left(\frac{3}{2}, \frac{r^2}{4\alpha}\right) = \int_0^{r^2/4\alpha} dt\sqrt{t}\exp(-t), \tag{1.5}$$

is the lower incomplete gamma function [56]. The classical Schwarzschild mass is recovered in the limit $r/\sqrt{\alpha} \to \infty$. It was shown that the coordinate noncommutativity cures the usual problems encountered in the description of the terminal phase of black hole evaporation. More specifically, it was found that the evaporation end-point is a zero temperature extremal black hole and there exist a finite maximum temperature that a black hole can reach before cooling down to absolute zero. The existence of a regular de Sitter at the origin's neighborhood was also shown, implying the absence of a curvature singularity at the origin. Recently, further research on noncommutative black holes has been undertaken, with new solutions found providing smeared source terms for charged and higher dimensional cases [58–62]. Furthermore, exact solutions of semi-classical wormholes [63, 64] in the context of noncommutative geometry were found [65], and their physical properties and characteristics were analyzed.

Despite the fact that both concepts have their own scale of observability, in particular, non-commutativeness manifests itself only at sufficiently high energies and small distances, and the gravastar concept is applicable to larger scales, one may argue that due to gravitational instabilities inhomogeneities may arise. Thus, the gravastar solutions outlined in this paper may possibly originate from density fluctuations in the cosmological background, resulting in the nucleation through the respective density perturbations.

This paper is outlined in the following manner. In section 2, we present the generic structure equations of gravastars, and specify the mass function in the context of noncommutative geometry. In section 3, the linearized stability analysis procedure is outlined, and the stability regions of the transition layer of gravastars are determined. Finally in section 5, we conclude. We adopt the convention $G = c = 1$ throughout this work.

2 Structure equations of gravastars in noncommutative geometry

2.1 Spacetime metric and field equations

Consider the interior spacetime, without a loss of generality, given by the following metric, in curvature coordinates

$$ds^2 = -e^{2\Phi(r)}\,dt^2 + \frac{dr^2}{1 - 2m(r)/r} + r^2\,d\Omega^2, \tag{2.1}$$

where $d\Omega^2 = (d\theta^2 + \sin^2\theta\,d\phi^2)$; $\Phi(r)$ and $m(r)$ are arbitrary functions of the radial coordinate, r. The function $m(r)$ is the quasi-local mass, and is denoted as the mass function.

JHEP12(2013)065

The Einstein field equation, $G_{\mu\nu} = 8\pi T_{\mu\nu}$ provides the following relationships

$$m' = 4\pi r^2 \rho \,, \tag{2.2}$$

$$\Phi' = \frac{m + 4\pi r^3 p_r}{r(r-2m)} \,, \tag{2.3}$$

$$p_r' = -\frac{(\rho + p_r)(m + 4\pi r^3 p_r)}{r(r-2m)} + \frac{2}{r}(p_t - p_r) \,, \tag{2.4}$$

where the prime denotes a derivative with respect to the radial coordinate. $\rho(r)$ is the energy density, $p_r(r)$ is the radial pressure, and $p_t(r)$ is the tangential pressure. Equation (2.4) corresponds to the anisotropic pressure Tolman-Oppenheimer-Volkoff (TOV) equation.

Using the equation of state, $p_r = -\rho$, and taking into account the field equations (2.2) and (2.3), we have the following relationship

$$\Phi'(r) = \frac{m - rm'}{r\,(r-2m)} \,, \tag{2.5}$$

which provides the solution given by

$$\Phi(r) = \frac{1}{2} \ln\left[1 - \frac{2m(r)}{r}\right] . \tag{2.6}$$

One now has at hand three equations, namely, the field eqs. (2.2)–(2.4), with four unknown functions of r, i.e., $\rho(r)$, $p_r(r)$, $p_t(r)$, and $m(r)$. We shall consider the approach by choosing a specific choice for a physically reasonable mass function $m(r)$, thus closing the system.

Despite the fact that one may consider the general line element given by eq. (1.2), and determine a generalized mass function, we emphasize that we have considered the analysis using curvature coordinates. Thus, in this context, we are interested in the noncommutative geometry inspired mass function given by eq. (1.4), in curvature coordinates. The latter is reorganized into the following form

$$m(r) = \frac{2M}{\sqrt{\pi}} \gamma\left(\frac{3}{2}, \beta\left(\frac{r}{2M}\right)^2\right) , \tag{2.7}$$

where β is defined as $\beta = M^2/\alpha$.

Note that three cases need to be analyzed [56]:

a) if $\beta < 1.9$, no roots are present;

b) if $\beta > 1.9$, we have two roots, r_- and r_+, with $r_+ > r_-$;

c) if $\beta = 1.9$, we have $r_+ = r_-$, which may be interpreted as an *extreme* situation, such as the extreme Reissner-Nordström metric.

The function $f(r) = (1 - 2m(r)/r)$ is depicted in figure 1 for these three cases for the following values $\beta = 1.5$, $\beta = 1.9$ and $\beta = 3.5$, respectively. Note that all the roots lie within the Schwarzschild radius $r_b = 2M$, where M is the total mass of the system.

JHEP12(2013)065

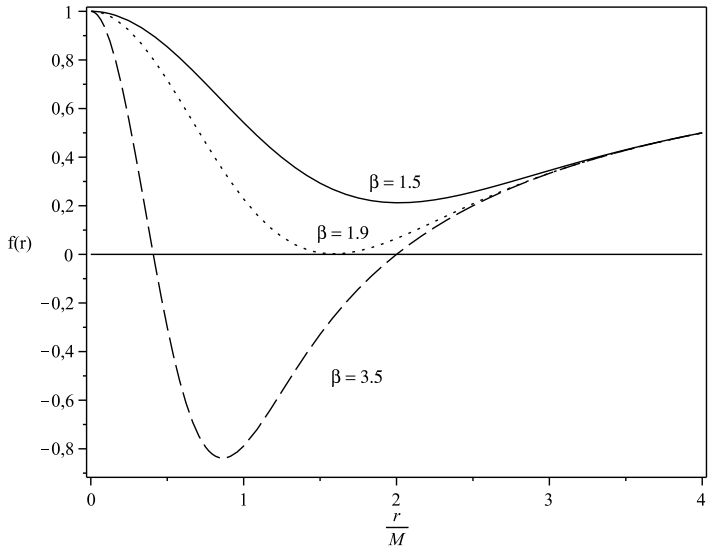

Figure 1. The function $f(r) = (1 - 2m(r)/r)$ is depicted for the three cases with the following values $\beta = 1.5$, $\beta = 1.9$ and $\beta = 3.5$, respectively.

Note that for the specific equation of state that yields the solution (2.6), the stress-energy profile is given by the following relationships

$$\rho(r) = -p_r(r) = \frac{1}{4\pi}\frac{m'(r)}{r^2}\,, \tag{2.8}$$

$$p_t(r) = \frac{1}{8\pi}\frac{m''(r)}{r}\,, \tag{2.9}$$

respectively. Taking into account the mass function given by eq. (2.7), these take the following form

$$\rho(r) = -p_r(r) = \frac{M}{(4\pi\alpha)^{3/2}}\exp\left(-\frac{r^2}{4\alpha}\right), \tag{2.10}$$

$$p_t(r) = \frac{M}{(4\pi\alpha)^{3/2}}\left(1-\frac{r^2}{4\alpha}\right)\exp\left(-\frac{r^2}{4\alpha}\right). \tag{2.11}$$

The stress-energy profile is qualitatively represented in figure 2. The plots are depicted in terms of dimensionless quantities, $M^2 p_r(r)$ and $M^2 p_t(r)$, respectively. Note that the radial pressure is essentially negative, taking extremely low negative values for high values of the parameter β and low values of the radial coordinate, and tends asymptotically to zero at spatial infinity. Note that as the equation of state $p_r(r) = -\rho(r)$ is assumed, the energy density is positive and tends to zero as $r \to \infty$. The tangential pressure, depicted in the right plot of figure 2, possesses a positive patch, but is also essentially negative throughout the spacetime geometry.

2.2 Gravitational collapse and gravity profile

In this work we analyse the linearized stability analysis around a stable solution, but it is also important to consider the instabilities which arise from the gravitational collapse of

JHEP12(2013)065

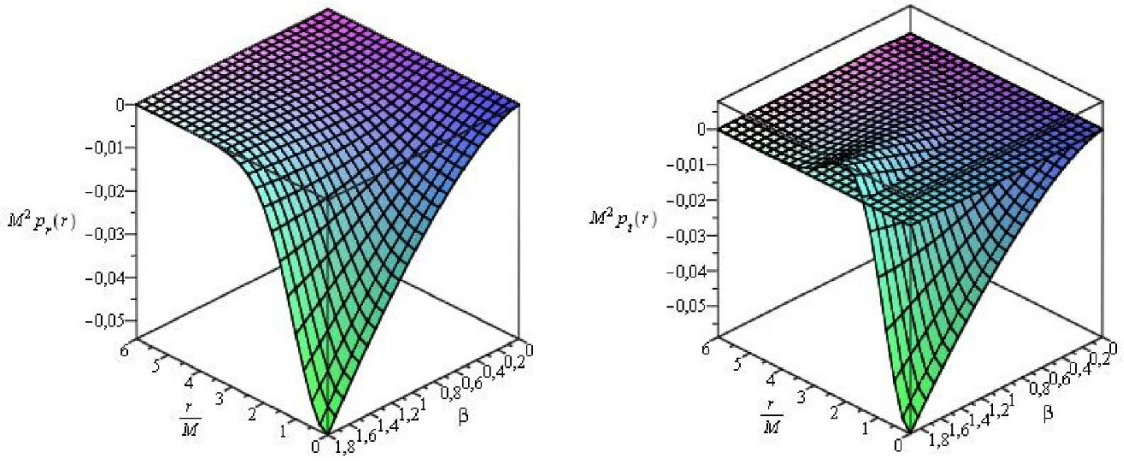

Figure 2. The stress-energy profile is represented in the plots, in terms of dimensionless quantities, $M^2 p_r(r)$ and $M^2 p_t(r)$, respectively. The radial pressure, depicted in the left plot, is essentially negative, taking extremely low negative values for high values of the parameter β and low values of the radial coordinate. The tangential pressure, depicted in the right plot, possesses a positive patch, but is also essentially negative throughout the spacetime geometry. See the text for more details.

the star. Note that, in particular, an expression for $m(r)$ is deduced, and it is not clear whether such a mass distribution can be maintained. It is generally believed that any star which crosses its Schwarzschild radius collapses due to gravitational attraction. Thus, it is important to comment on the mechanism which prevents such a collapse.

To this effect, consider the locally measured acceleration due to gravity, given by the following relationship: $\mathcal{A} = \sqrt{1-2m(r)/r}\,\Phi'(r)$ [17], where the factor $\Phi'(r)$ may be considered the "gravity profile". Now, the convention used is that $\Phi'(r)$ is positive for an inwardly gravitational attraction, and negative for an outward gravitational repulsion. The gravity profile $\Phi'(r)$ is plotted in figure 3. Note that for large values of the radial coordinate and large values of the parameter β, the gravity profile is positive, implying an attractive nature of the geometry.

However, one encounters a repulsive nature of the spacetime geometry, as $\Phi' < 0$, for the following cases: (i) low values of the radial coordinate, especially in the range of $0.5 \leq \beta < 1.9$; (ii) for arbitrary values of r, in the range $\beta \leq 0.5$. In this context, one may argue that due to the gravitational collapse of the star, the matter does not cross the Schwarzschild horizon due to the repulsive character of the spacetime, and it is possible that an equilibrium stability region is attained. Thus, it is the repulsive character of the geometry that stops the gravitational collapse from crossing the Schwarzschild horizon and that sustains this gravastar configuration.

3 Thin-shell formalism

The thin-shell is not necessary for all solutions. In fact, the original Maur-Mottola gravastar picture considered a finite thick shell of stiff matter, $p = \rho$, situated near where the event

JHEP12(2013)065

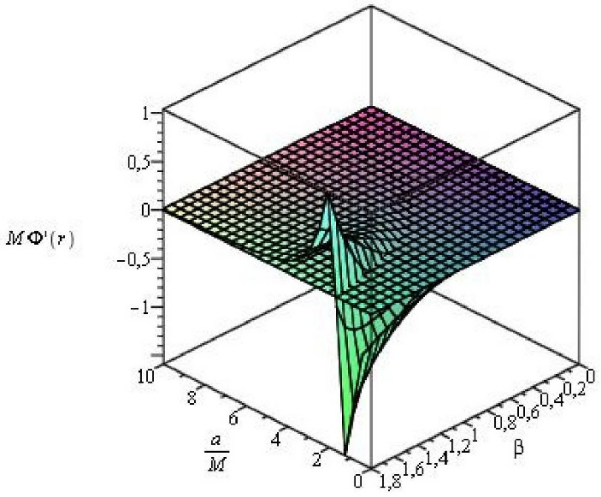

Figure 3. Depicted is the dimensionless quantity for the "gravity profile", $M\Phi'(r)$. The latter is positive for an inwardly gravitational attraction and negative for an outwardly gravitational repulsion. One verifies qualitatively from the plot that $\Phi' > 0$ for values of $0.5 \leq \beta < 1.9$, rendering the geometry attractive in this range. The geometry possesses a repulsive character for a wide range of values of the radial coordinate and for $\beta \leq 0.5$. In this context, we argue that this repulsive nature of the geometry stops the gravitational collapse from crossing the Schwarzschild horizon. Thus, it is possible that an equilibrium stability region is attained. See the text for details.

horizon is expected to form. However, considering an idealization of a thin shell, one may simplify considerably the dynamic stability analysis of the setup, in particular, consider the linearized stability analysis outlined in the present work. Indeed, the simplified model considered shares the key features of the Mazur-Mottola scenario, and is sufficiently simple to be amenable to a full dynamical analysis.

3.1 Exterior spacetime

We shall model specific gravastar geometries by matching an interior gravastar geometry, given by eq. (2.1), where the metric functions are given by eqs. (2.6) and (2.7), with an exterior Schwarzschild solution

$$ds^2 = -\left(1 - \frac{2M}{r}\right) dt^2 + \left(1 - \frac{2M}{r}\right)^{-1} dr^2 + r^2 \left(d\theta^2 + \sin^2\theta \, d\phi^2\right), \tag{3.1}$$

at a junction interface Σ, situated outside the event horizon, $a > r_b = 2M$. We emphasize that the larger root r_+ lies inside the Schwarzschild event horizon. More specifically, if one considers the case $\beta > 1.9$, one would have two roots, i.e., two event horizons lying within the Schwarzschild radius. Thus, in this work we are only interested in the case of $\beta < 1.9$, which corresponds to the absence of event horizons for the inner solution. This is in order to have a gravastar solution without an event horizon, as its rigid surface is located at a radius slightly greater than the Schwarzschild radius.

JHEP12(2013)065

3.2 Junction interface

Consider the junction surface Σ as a timelike hypersurface defined by the parametric equation of the form $f(x^\mu(\xi^i)) = 0$. $\xi^i = (\tau, \theta, \phi)$ are the intrinsic coordinates on Σ, where τ is the proper time on the hypersurface. The three basis vectors tangent to Σ are given by $e_{(i)} = \partial/\partial\xi^i$, with the following components $e^\mu_{(i)} = \partial x^\mu/\partial\xi^i$. The induced metric on the junction surface is then provided by the scalar product $g_{ij} = e_{(i)} \cdot e_{(j)} = g_{\mu\nu} e^\mu_{(i)} e^\nu_{(j)}$. Thus, the intrinsic metric to Σ is given by

$$ds^2_\Sigma = -d\tau^2 + a^2 \left(d\theta^2 + \sin^2\theta \, d\phi^2\right). \tag{3.2}$$

Note that the junction surface, $r = a$, is situated outside the event horizon, i.e., $a > r_b$, to avoid a black hole solution, and we are only interested in the case of $\beta < 1.9$, of eq. (2.7), as emphasized above.

For the specific cases considered in this work, namely, the interior and exterior spacetimes given by eqs. (2.1) and (3.1), respectively, the four-velocity of the junction surface $x^\mu(\tau, \theta, \phi) = (t(\tau), a(\tau), \theta, \phi)$ is given by

$$U^\mu_\pm = \left(\frac{dt}{d\tau}, \frac{da}{d\tau}, 0, 0\right) = \left(\frac{\sqrt{1 - \frac{2m_\pm}{a} + \dot{a}^2}}{1 - \frac{2m_\pm}{a}}, \dot{a}, 0, 0\right), \tag{3.3}$$

where the overdot denotes a derivative with respect to the proper time, τ. The $(\pm)$ superscripts correspond to the exterior and interior spacetimes, respectively, so that $m_\pm$ are defined as $m_- = m(a)$ and $m_+ = M$, respectively.

The unit normal 4−vector, n^μ, to Σ is defined as

$$n_\mu = \pm \left| g^{\alpha\beta} \frac{\partial f}{\partial x^\alpha} \frac{\partial f}{\partial x^\beta} \right|^{-1/2} \frac{\partial f}{\partial x^\mu}, \tag{3.4}$$

with $n_\mu n^\mu = +1$ and $n_\mu e^\mu_{(i)} = 0$. The Israel formalism requires that the normals point from the interior spacetime to the exterior spacetime [66–69]. Thus, for the interior and exterior spacetimes given by the metrics (2.1) and (3.1), respectively, the normals may be determined from eq. (3.4), or from the contractions $U^\mu n_\mu = 0$ and $n^\mu n_\mu = +1$, and are provided by

$$n^\pm_\mu = \left(-\dot{a}, \frac{\sqrt{1 - \frac{2m_\pm}{a} + \dot{a}^2}}{1 - \frac{2m_\pm}{a}}, 0, 0\right), \tag{3.5}$$

respectively, with $m_\pm$ defined as $m_- = m(a)$ and $m_+ = M$, as before.

3.3 Extrinsic curvature

The extrinsic curvature is defined as $K_{ij} = n_{\mu;\nu} e^\mu_{(i)} e^\nu_{(j)}$. Differentiating $n_\mu e^\mu_{(i)} = 0$ with respect to ξ^j, we have $n_\mu \frac{\partial^2 x^\mu}{\partial\xi^i \partial\xi^j} = -n_{\mu,\nu} \frac{\partial x^\mu}{\partial\xi^i} \frac{\partial x^\nu}{\partial\xi^j}$, so that the extrinsic curvature is finally given by

$$K^\pm_{ij} = -n_\mu \left(\frac{\partial^2 x^\mu}{\partial\xi^i \partial\xi^j} + \Gamma^{\mu\pm}_{\alpha\beta} \frac{\partial x^\alpha}{\partial\xi^i} \frac{\partial x^\beta}{\partial\xi^j}\right). \tag{3.6}$$

JHEP12(2013)065

Note that, in general, K_{ij} is not continuous across Σ, so that for notational convenience, the discontinuity in the extrinsic curvature is defined as $\kappa_{ij} = K^{+}_{ij} - K^{-}_{ij}$.

Taking into account the interior spacetime metric (2.1) and the Schwarzschild solution (3.1), the non-trivial components of the extrinsic curvature are given by

$$K^{\tau}{}_{\tau}{}^{+} = \frac{\frac{M}{a^2} + \ddot{a}}{\sqrt{1 - \frac{2M}{a} + \dot{a}^2}}\,, \tag{3.7}$$

$$K^{\tau}{}_{\tau}{}^{-} = \frac{\frac{m}{a^2} - \frac{m'}{a} + \ddot{a}}{\sqrt{1 - \frac{2m(a)}{a} + \dot{a}^2}}\,, \tag{3.8}$$

and

$$K^{\theta}{}_{\theta}{}^{+} = \frac{1}{a}\sqrt{1 - \frac{2M}{a} + \dot{a}^2}\,, \tag{3.9}$$

$$K^{\theta}{}_{\theta}{}^{-} = \frac{1}{a}\sqrt{1 - \frac{2m(a)}{a} + \dot{a}^2}\,, \tag{3.10}$$

respectively. The prime henceforth shall denote a derivative with respect to a.

3.4 Lanczos equation and surface stresses

The Einstein equations may be written in the following form,

$$S^{i}{}_{j} = -\frac{1}{8\pi}\left(\kappa^{i}{}_{j} - \delta^{i}{}_{j}\kappa^{k}{}_{k}\right), \tag{3.11}$$

denoted as the Lanczos equations, where $S^{i}{}_{j}$ is the surface stress-energy tensor on Σ. Considerable simplifications occur due to spherical symmetry, namely $\kappa^{i}{}_{j} = \mathrm{diag}(\kappa^{\tau}{}_{\tau}, \kappa^{\theta}{}_{\theta}, \kappa^{\theta}{}_{\theta})$. The surface stress-energy tensor may be written in terms of the surface energy density, σ, and the surface pressure, $\mathcal{P}$, as $S^{i}{}_{j} = \mathrm{diag}(-\sigma, \mathcal{P}, \mathcal{P})$. Thus, the Lanczos equation, eq. (3.11), then provide us with the following expressions for the surface stresses

$$\sigma = -\frac{1}{4\pi a}\left(\sqrt{1 - \frac{2M}{a} + \dot{a}^2} - \sqrt{1 - \frac{2m}{a} + \dot{a}^2}\right), \tag{3.12}$$

$$\mathcal{P} = \frac{1}{8\pi a}\left[\frac{1 - \frac{M}{a} + \dot{a}^2 + a\ddot{a}}{\sqrt{1 - \frac{2M}{a} + \dot{a}^2}} - \frac{1 - \frac{m}{a} - m' + \dot{a}^2 + a\ddot{a}}{\sqrt{1 - \frac{2m}{a} + \dot{a}^2}}\right]. \tag{3.13}$$

3.5 Energy conditions on the junction surface

It is interesting to consider whether the surface stresses, given by eqs. (3.12)–(3.13) satisfy the energy conditions on the thin-shell. We shall only consider the weak energy condition (WEC) and the null energy condition (NEC). The WEC implies $\sigma \geq 0$ and $\sigma + \mathcal{P} \geq 0$, and by continuity implies the null energy condition (NEC), $\sigma + \mathcal{P} \geq 0$. These will be evaluated for a static solution at a_0.

Taking into account eqs. (3.12)–(3.13), then the NEC is given by

$$\sigma + \mathcal{P} = \frac{1}{8\pi a_0}\left[\frac{1 - \frac{3m_0}{a_0} + m'(a_0)}{\sqrt{1 - \frac{2m(a_0)}{a_0}}} - \frac{1 - \frac{3M}{a_0}}{\sqrt{1 - \frac{2M}{a_0}}}\right], \tag{3.14}$$

JHEP12(2013)065

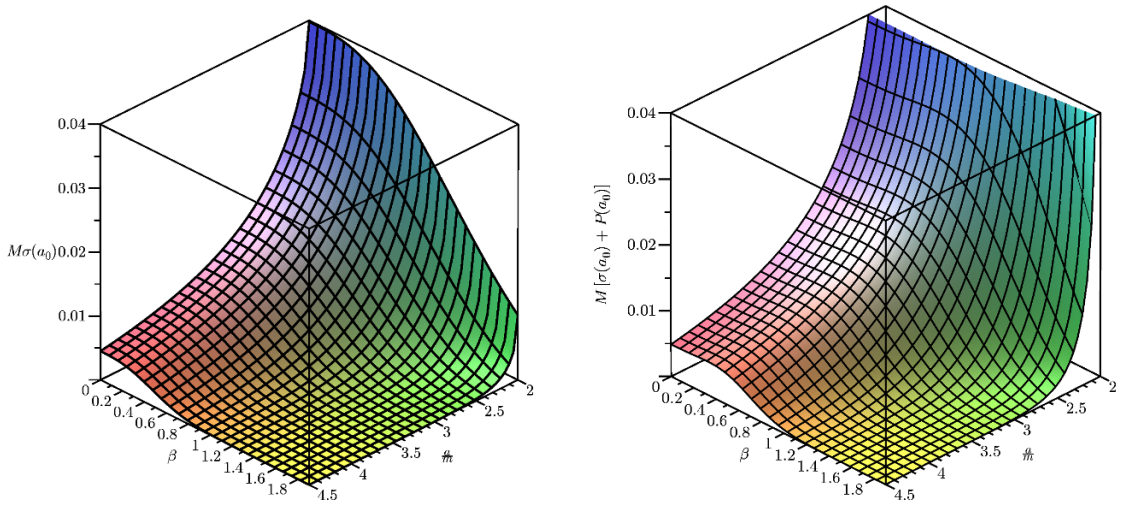

Figure 4. The weak energy condition (WEC) and the null energy condition (NEC) profiles are represented in the plots, in terms of dimensionless quantities, i.e., $M\sigma(a_0)$ and $M(\sigma(a_0)+\mathcal{P}(a_0))$. We verify that both quantiites are positive, consequently satisfying the WEC and NEC. See the text for more details.

where the mass function, evaluated at the junction interface a_0, is given by eq. (2.7). In order to verify whether the NEC and the WEC are satisfied, we plot the latter using the following dimensionless quantities: $M\sigma(a_0)$ and $M[\sigma(a_0)+\mathcal{P}(a_0)]$. We verify from figure 4, both quantities are positive throughout the spacetime, thus satisfying the WEC and NEC on the thin-shell.

3.6 Conservation identity

We also use the conservation identity given by $S^i_{j|i} = \left[T_{\mu\nu}e^{\mu}_{(j)}n^{\nu}\right]^+_-$, where $[X]^+_-$ denotes the discontinuity across the surface interface, i.e., $[X]^+_- = X^+|_\Sigma - X^-|_\Sigma$. The conservation identity is given by

$$\left[T_{\mu\nu}\, e^{\mu}_{(\tau)}\, n^{\nu}\right]^+_- = \left[T_{\mu\nu}\, U^{\mu}\, n^{\nu}\right]^+_- = \left[\left(-T^t{}_t + T^r{}_r\right)\frac{\dot{a}\sqrt{1-\frac{b(a)}{a}+\dot{a}^2}}{1-\frac{b(a)}{a}}\right]^+_-, \tag{3.15}$$

where $T^t{}_t$ and $T^r{}_r$ are the stress-energy tensor components, in the interior and exterior spacetimes. The momentum flux term in the right hand side corresponds to the net discontinuity in the momentum flux $F_\mu = T_{\mu\nu}\,U^\nu$ which impinges on the shell. The conservation identity is a statement that all energy and momentum that plunges into the thin shell, gets caught by the latter and converts into conserved energy and momentum of the surface stresses of the junction.

For the present case, note that $-T^t{}_t + T^r{}_r = \rho(r) + p_r(r) = 0$ in the interior spacetime and $T^t{}_t = T^r{}_r = 0$ in the exterior vacuum Schwarzschild geometry, so that the momentum flux is zero, i.e., $\left[T_{\mu\nu}e^{\mu}_{(j)}n^{\nu}\right]^+_- = 0$. We refer the reader to refs. [70, 71] for a more detailed analysis. Thus, the conservation identity reduces to the following conservation law $S^i_{j|i} = 0$.

JHEP12(2013)065

Note that $S^{i}_{\tau|i} = -[\dot{\sigma} + 2\dot{a}(\sigma + \mathcal{P})/a]$, so that the conservation identity provides us with

$$\sigma' = -\frac{2}{a}(\sigma + \mathcal{P})\,. \tag{3.16}$$

This relationship will be used in the linearized stability analysis considered below.

Consider that $A = 4\pi a^2$ is the surface area of the thin shell, so that the conservation equation provides the following relationship

$$\frac{d(\sigma A)}{d\tau} + \mathcal{P}\frac{dA}{d\tau} = 0\,. \tag{3.17}$$

The first term represents the variation of the internal energy of the shell, the second term is the work done by the shell's internal force.

4 Linearized stability analysis

4.1 Equation of motion

Equation (3.12) may be rearranged to provide the thin shell's equation of motion given by the following relationship

$$\dot{a}^2 + V(a) = 0\,. \tag{4.1}$$

The potential is given by

$$V(a) = F(a) - \left[\frac{m_s(a)}{2a}\right]^2 - \left[\frac{aG(a)}{m_s(a)}\right]^2, \tag{4.2}$$

where, for notational convenience, the factors $F(a)$ and $G(a)$ are defined as

$$F(a) = 1 - \frac{m(a) + M}{a}\,, \tag{4.3}$$

$$G(a) = \frac{M - m(a)}{a}\,. \tag{4.4}$$

Linearizing around a stable solution situated at a_0, we consider a Taylor expansion of $V(a)$ around a_0 to second order, given by

$$V(a) = V(a_0) + V'(a_0)(a - a_0) + \frac{1}{2}V''(a_0)(a - a_0)^2 + O[(a - a_0)^3]\,. \tag{4.5}$$

The first and second derivatives of $V(a)$ are given by

$$V'(a) = F' - 2\left(\frac{m_s}{2a}\right)\left(\frac{m_s}{2a}\right)' - 2\left(\frac{aG}{m_s}\right)\left(\frac{aG}{m_s}\right)' \tag{4.6}$$

$$V''(a) = F'' - 2\left[\left(\frac{m_s}{2a}\right)'\right]^2 - 2\left(\frac{m_s}{2a}\right)\left(\frac{m_s}{2a}\right)'' - 2\left[\left(\frac{aG}{m_s}\right)'\right]^2 - 2\left(\frac{aG}{m_s}\right)\left(\frac{aG}{m_s}\right)'', \tag{4.7}$$

respectively.

JHEP12(2013)065

Evaluated at the static solution, at $a = a_0$, so that $\dot{a} = \ddot{a} = 0$, we verify that $V(a_0) = 0$ and $V'(a_0) = 0$. From the condition $V'(a_0) = 0$, one extracts the following useful equilibrium relationship

$$\Gamma \equiv \left(\frac{m_s}{2a_0}\right)' = \left(\frac{a_0}{m_s}\right)\left[F' - 2\left(\frac{a_0 G}{m_s}\right)\left(\frac{a_0 G}{m_s}\right)'\right], \tag{4.8}$$

which will be used in determining the master equation, responsible for dictating the stable equilibrium configurations.

4.2 Parametrization of the stable equilibrium

Using the surface mass of the thin shell $m_s = 4\pi a^2 \sigma$, the conservation law of the surface stresses, i.e., eq. (3.16), can be rearranged to provide the following relationship

$$\left(\frac{m_s}{2a}\right)'' = \Upsilon - 4\pi\sigma'\eta\,, \tag{4.9}$$

with the parameter η defined as $\eta = \mathcal{P}'/\sigma'$, and for notational simplicity, the function Υ is given by

$$\Upsilon \equiv \frac{4\pi}{a}\left(\sigma + \mathcal{P}\right). \tag{4.10}$$

Equation (4.9) will play a fundamental role in determining the stability regions of the respective solutions. Note that η is used as a parametrization of the stable equilibrium, so that there is no need to specify a surface equation of state. The parameter $\sqrt{\eta}$ is normally interpreted as the speed of sound, so that one would expect that $0 < \eta \leq 1$, based on the requirement that the speed of sound should not exceed the speed of light. We refer the reader to refs. [49, 50] for further discussions on the respective physical interpretation of η lying outside the range $0 < \eta \leq 1$.

The solution is stable if and only if $V(a)$ has a local minimum at a_0 and $V''(a_0) > 0$ is verified. Thus, from the latter stability condition, after a rather lengthy but straightforward calculation, one deduces the master equation for the stability regions, given by

$$\eta_0 \left.\frac{d\sigma^2}{da}\right|_{a_0} > \Theta\,, \tag{4.11}$$

where $\eta_0 = \eta(a_0)$. Note that to deduce this inequality, we have used eq. (4.9), and for notational simplicity, we have defined the function Θ by

$$\Theta \equiv \frac{1}{2\pi}\left[\sigma\Upsilon + \frac{1}{2\pi a_0}(\Gamma^2 - \Psi)\right], \tag{4.12}$$

with Γ given by eq. (4.8), and the function Ψ defined as

$$\Psi = \frac{F''}{2} - \left[\left(\frac{aG}{m_s}\right)'\right]^2 - \left(\frac{aG}{m_s}\right)\left(\frac{aG}{m_s}\right)''. \tag{4.13}$$

JHEP12(2013)065

Now, from the master inequality (4.11), we find that the stable equilibrium regions are dictated by the following inequalities

$$\eta_0 > \Omega\,, \qquad \text{if} \qquad \frac{d\sigma^2}{da}\Big|_{a_0} > 0\,, \tag{4.14}$$

$$\eta_0 < \Omega\,, \qquad \text{if} \qquad \frac{d\sigma^2}{da}\Big|_{a_0} < 0\,, \tag{4.15}$$

with the definition

$$\Omega \equiv \Theta\left(\frac{d\sigma^2}{da}\Big|_{a_0}\right)^{-1}. \tag{4.16}$$

4.3 Stability regions

We now determine the stability regions dictated by the inequalities (4.14)–(4.15). In the specific cases that follow, the explicit form of Ω is extremely messy, so that we find it more instructive to show the stability regions graphically.

For the case of interest under consideration, namely, $\beta < 1.9$, the specific expression for $d\sigma^2/da|_{a_0}$ is given by

$$\begin{aligned}\frac{d\sigma^2}{da}\Big|_{a_0} = \frac{1}{8\pi a^4}&\left[\frac{\sqrt{1-\frac{2M}{a}}-\sqrt{1-\frac{2m(a)}{a}}}{\sqrt{1-\frac{2M}{a}}\sqrt{1-\frac{2m(a)}{a}}}\right]\times\\ &\times\left\{[a-3m(a)+am'(a)]\sqrt{1-\frac{2M}{a}}-(a-3M)\sqrt{1-\frac{2m(a)}{a}}\right\}.\end{aligned} \tag{4.17}$$

It is useful to consider the dimensionless quantity $M^3 d\sigma^2/da|_{a_0}$, which is depicted in figure 5. From the latter, it is transparent that $d\sigma^2/da|_{a_0} < 0$, so that the stability regions are dictated by inequality (4.15).

The respective stability regions are given by the plot depicted below the surface in figure 6. It is interesting to note that the stability regions are sufficiently close to where the event horizon is expected to form, which is extremely promising. Indeed, large stability stability regions exist in the neighbourhood of where the event horizon is expected to form, for arbitrary values of the parameter β. For low values of the parameter, the stability regions decrease for increasing values of a. For large values of β the stability regions decrease for increasing values a, and then increase again as a increases. Thus large stability regions exist also for large values of β, for regions sufficiently far from the where the event horizon is expected to form.

The message that one may extract, is that the above analysis shows that stable configurations of the surface layer, located sufficiently near to where the event horizon is expected to form, do indeed exist. Therefore, considering these models, one may conclude that the exterior geometry of a noncommutative geometry inspired gravastar would be practically indistinguishable from a black hole.

JHEP12(2013)065

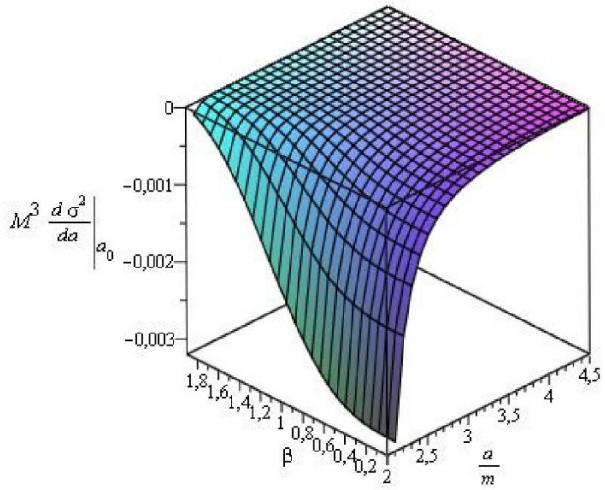

Figure 5. The sign of the dimensionless quantity $M^3 d\sigma^2/da|_{a_0}$ is depicted in the plot, where it is transparent that $d\sigma^2/da|_{a_0} < 0$. Thus, the stability regions are dictated by inequality (4.15). See the text for more details.

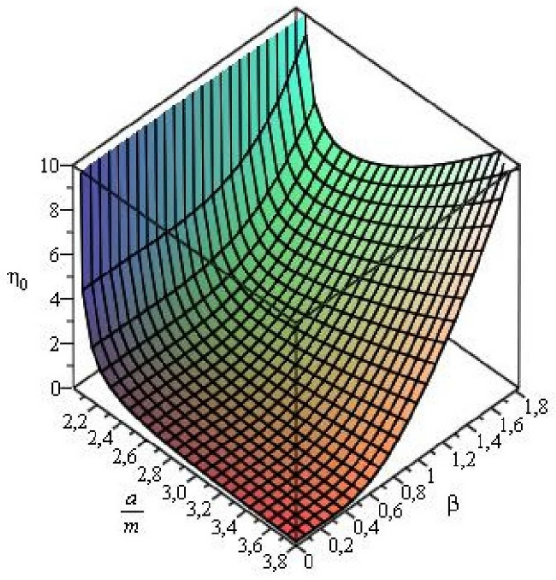

Figure 6. The respective stability regions are given by the plot depicted below the surface. Large stability stability regions exist in the neighbourhood of where the event horizon is expected to form, for arbitrary values of the parameter β. For low values of the parameter, the stability regions decrease for increasing values of a. For large values of β the stability regions decrease for increasing values a, and then increase again as a increases. See the text for more details.

5 Summary and conclusion

The gravastar model was proposed as an alternative picture for the final state of gravitational collapse. It remains an open problem if alternatives to standard black holes as the final state of gravitational collapse do really exist and only a full quantum theory of gravity

JHEP12(2013)065

could answer this question adequately. This justifies the research on black hole mimickers that could explain observational data without the paradoxical problems regarding black holes.

In this work, we have found exact gravastar solutions in the context of noncommutative geometry, and briefly explored their physical properties and characteristics. More specifically, the energy density of these geometries is a smeared and particle-like gravitational source, where the mass is diffused throughout a region of linear dimension $\sqrt{\alpha}$ due to the intrinsic uncertainty encoded in the coordinate commutator. Furthermore, the mass function was deduced from the Einstein field equations, and the equation of state $p_r(r) = -\rho(r)$ was imposed.

A fundamental aim in this work was to analyse the linearized stability analysis of the transition layer of these noncommutative geometry inspired gravastars around static equilibrium solutions. However, it is also important to consider the instabilities which arise from the gravitational collapse of the star. It is generally believed that any star crosses its Schwarzschild radius collapses due to gravitational attraction. Therefore, we have also commented on a mechanism which prevents such a collapse. We have shown that the spacetime has a repulsive character for a wide range of the parameters of the model. Therefore, we have argued that it is the repulsive nature of the geometry that stops the gravitational collapse of the star, and it is possible that an equilibrium stability region is attained, thus sustaining this gravastar configuration.

We further explored the dynamical stability of the transition layer of these noncommutative geometry inspired gravastars to linearized spherically symmetric radial perturbations about static equilibrium solutions. More specifically, we considered the speed of sound parameter η defined as $\eta = \mathcal{P}'/\sigma'$, where ρ and $\mathcal{P}$, are the surface energy density and surface pressure, respectively. The parameter η was used as a parametrization of the stable equilibrium, so that there was no need to specify a surface equation of state. Consequently, a master equation was deduced that dictated the stability regions. It was found that large stability regions do exist, which are located sufficiently close to where the event horizon is expected to form, for a wide range of the parameters of the model. Thus, it would be difficult to distinguish the exterior geometry of the gravastars, analyzed in this work, from a black hole.

Indeed, in this work, we were only interested in the linearized spherically symmetric radial perturbations of the transition layer around static equilibrium solutions. However, we note that a thorough stability analysis of the whole system is in order to verify the stability of the entire gravastar configuration. To this effect, one may consider the non-spherically symmetric stability analysis explored in ref. [72], where general axial perturbations and monopole-type polar perturbations were considered in the linear approximation, for two classes of solutions, namely, wormholes with flat asymptotic behavior at one end and AdS on the other (M-AdS wormholes) and regular black holes with asymptotically de Sitter expansion far beyond the horizon (the so-called black universes). As a result of the analysis, it was shown that all configurations under study are unstable under spherically symmetric perturbations, except for a special class of black universes where the event horizon coincides with the minimum of the area function. It will be interesting to apply the stability analysis

JHEP12(2013)065

outlined in ref. [72] to the entire gravastar configuration, which we leave for a future publication.

In conclusion, it would be interesting to apply to the present case, the alternative formalism developed in two companion papers [70, 71], where an extremely general and robust framework leading to the linearized stability analysis of dynamical spherically symmetric thin-shell gravastars was developed. In the latter, the logic flow was reversed, where the surface mass as a function of the potential was considered, so that specifying the latter informs on how much surface mass one needs to put on the transition layer. Work along these lines is currently underway.

Acknowledgments

FSNL acknowledges partial financial support of the Fundação para a Ciência e Tecnologia through the grants CERN/FP/123615/2011 and CERN/FP/123618/2011.

References

[1] P.O. Mazur and E. Mottola, *Gravitational condensate stars: an alternative to black holes*, gr-qc/0109035 [INSPIRE].

[2] P.O. Mazur and E. Mottola, *Dark energy and condensate stars: Casimir energy in the large*, gr-qc/0405111 [INSPIRE].

[3] P.O. Mazur and E. Mottola, *Gravitational vacuum condensate stars*, *Proc. Nat. Acad. Sci.* **101** (2004) 9545 [gr-qc/0407075] [INSPIRE].

[4] G. Chapline, E. Hohlfeld, R.B. Laughlin and D.I. Santiago, *Quantum phase transitions and the breakdown of classical general relativity*, *Int. J. Mod. Phys.* **A 18** (2003) 3587 [gr-qc/0012094] [INSPIRE].

[5] G. Chapline, *Dark energy stars*, *eConf* **C 041213** (2004) 0205 [astro-ph/0503200] [INSPIRE].

[6] F.S.N. Lobo, *Stable dark energy stars*, *Class. Quant. Grav.* **23** (2006) 1525 [gr-qc/0508115] [INSPIRE].

[7] M. Visser and D.L. Wiltshire, *Stable gravastars: an alternative to black holes?*, *Class. Quant. Grav.* **21** (2004) 1135 [gr-qc/0310107] [INSPIRE].

[8] B.M.N. Carter, *Stable gravastars with generalised exteriors*, *Class. Quant. Grav.* **22** (2005) 4551 [gr-qc/0509087] [INSPIRE].

[9] P. Rocha, R. Chan, M.F.A. da Silva and A. Wang, *Stable and 'bounded excursion' gravastars and black holes in Einstein's theory of gravity*, *JCAP* **11** (2008) 010 [arXiv:0809.4879] [INSPIRE].

[10] C. Cattoen, T. Faber and M. Visser, *Gravastars must have anisotropic pressures*, *Class. Quant. Grav.* **22** (2005) 4189 [gr-qc/0505137] [INSPIRE].

[11] A. DeBenedictis, D. Horvat, S. Ilijic, S. Kloster and K.S. Viswanathan, *Gravastar solutions with continuous pressures and equation of state*, *Class. Quant. Grav.* **23** (2006) 2303 [gr-qc/0511097] [INSPIRE].

[12] F.S.N. Lobo and A.V.B. Arellano, *Gravastars supported by nonlinear electrodynamics*, *Class. Quant. Grav.* **24** (2007) 1069 [gr-qc/0611083] [INSPIRE].

JHEP12(2013)065

[13] N. Bilic, G.B. Tupper and R.D. Viollier, *Born-Infeld phantom gravastars*, *JCAP* **02** (2006) 013 [astro-ph/0503427] [INSPIRE].

[14] A. DeBenedictis, R. Garattini and F.S.N. Lobo, *Phantom stars and topology change*, *Phys. Rev.* **D 78** (2008) 104003 [arXiv:0808.0839] [INSPIRE].

[15] O. Bertolami and J. Paramos, *The Chaplygin dark star*, *Phys. Rev.* **D 72** (2005) 123512 [astro-ph/0509547] [INSPIRE].

[16] S.S. Yazadjiev, *Exact dark energy star solutions*, *Phys. Rev.* **D 83** (2011) 127501 [arXiv:1104.1865] [INSPIRE].

[17] F.S.N. Lobo, *Van der Waals quintessence stars*, *Phys. Rev.* **D 75** (2007) 024023 [gr-qc/0610118] [INSPIRE].

[18] A.E. Broderick and R. Narayan, *Where are all the gravastars? Limits upon the gravastar model from accreting black holes*, *Class. Quant. Grav.* **24** (2007) 659 [gr-qc/0701154] [INSPIRE].

[19] C.B.M.H. Chirenti and L. Rezzolla, *How to tell a gravastar from a black hole*, *Class. Quant. Grav.* **24** (2007) 4191 [arXiv:0706.1513] [INSPIRE].

[20] D. Horvat and S. Ilijic, *Gravastar energy conditions revisited*, *Class. Quant. Grav.* **24** (2007) 5637 [arXiv:0707.1636] [INSPIRE].

[21] V. Cardoso, P. Pani, M. Cadoni and M. Cavaglia, *Ergoregion instability of ultracompact astrophysical objects*, *Phys. Rev.* **D 77** (2008) 124044 [arXiv:0709.0532] [INSPIRE].

[22] C.B.M.H. Chirenti and L. Rezzolla, *On the ergoregion instability in rotating gravastars*, *Phys. Rev.* **D 78** (2008) 084011 [arXiv:0808.4080] [INSPIRE].

[23] D. Horvat, S. Ilijic and A. Marunovic, *Electrically charged gravastar configurations*, *Class. Quant. Grav.* **26** (2009) 025003 [arXiv:0807.2051] [INSPIRE].

[24] B.V. Turimov, B.J. Ahmedov and A.A. Abdujabbarov, *Electromagnetic fields of slowly rotating magnetized gravastars*, *Mod. Phys. Lett.* **A 24** (2009) 733 [arXiv:0902.0217] [INSPIRE].

[25] T. Harko, Z. Kovacs and F.S.N. Lobo, *Can accretion disk properties distinguish gravastars from black holes?*, *Class. Quant. Grav.* **26** (2009) 215006 [arXiv:0905.1355] [INSPIRE].

[26] E. Mottola, *New horizons in gravity: the trace anomaly, dark energy and condensate stars*, *Acta Phys. Polon.* **B 41** (2010) 2031 [arXiv:1008.5006] [INSPIRE].

[27] J.P.S. Lemos, F.S.N. Lobo and S. Quinet de Oliveira, *Morris-Thorne wormholes with a cosmological constant*, *Phys. Rev.* **D 68** (2003) 064004 [gr-qc/0302049] [INSPIRE].

[28] S.V. Sushkov, *Wormholes supported by a phantom energy*, *Phys. Rev.* **D 71** (2005) 043520 [gr-qc/0502084] [INSPIRE].

[29] F.S.N. Lobo, *Phantom energy traversable wormholes*, *Phys. Rev.* **D 71** (2005) 084011 [gr-qc/0502099] [INSPIRE].

[30] E.F. Eiroa, *Stability of thin-shell wormholes with spherical symmetry*, *Phys. Rev.* **D 78** (2008) 024018 [arXiv:0805.1403] [INSPIRE].

[31] F.S.N. Lobo, *Surface stresses on a thin shell surrounding a traversable wormhole*, *Class. Quant. Grav.* **21** (2004) 4811 [gr-qc/0409018] [INSPIRE].

[32] F.S.N. Lobo, *Energy conditions, traversable wormholes and dust shells*, *Gen. Rel. Grav.* **37** (2005) 2023 [gr-qc/0410087] [INSPIRE].

JHEP12(2013)065

[33] J.P.S. Lemos and F.S.N. Lobo, *Plane symmetric traversable wormholes in an anti-de Sitter background*, *Phys. Rev.* **D 69** (2004) 104007 [gr-qc/0402099] [INSPIRE].

[34] F.S.N. Lobo, *Exotic solutions in general relativity: traversable wormholes and 'warp drive' spacetimes*, arXiv:0710.4474 [INSPIRE].

[35] P.R. Brady, J. Louko and E. Poisson, *Stability of a shell around a black hole*, *Phys. Rev.* **D 44** (1991) 1891 [INSPIRE].

[36] M. Ishak and K. Lake, *Stability of transparent spherically symmetric thin shells and wormholes*, *Phys. Rev.* **D 65** (2002) 044011 [gr-qc/0108058] [INSPIRE].

[37] E.F. Eiroa and G.E. Romero, *Linearized stability of charged thin shell wormholes*, *Gen. Rel. Grav.* **36** (2004) 651 [gr-qc/0303093] [INSPIRE].

[38] F.S.N. Lobo and P. Crawford, *Stability analysis of dynamic thin shells*, *Class. Quant. Grav.* **22** (2005) 4869 [gr-qc/0507063] [INSPIRE].

[39] F.S.N. Lobo, *Stability of phantom wormholes*, *Phys. Rev.* **D 71** (2005) 124022 [gr-qc/0506001] [INSPIRE].

[40] E.F. Eiroa and C. Simeone, *Cylindrical thin shell wormholes*, *Phys. Rev.* **D 70** (2004) 044008 [gr-qc/0404050] [INSPIRE].

[41] E.F. Eiroa and C. Simeone, *Thin-shell wormholes in dilaton gravity*, *Phys. Rev.* **D 71** (2005) 127501 [gr-qc/0502073] [INSPIRE].

[42] M. Thibeault, C. Simeone and E.F. Eiroa, *Thin-shell wormholes in Einstein-Maxwell theory with a Gauss-Bonnet term*, *Gen. Rel. Grav.* **38** (2006) 1593 [gr-qc/0512029] [INSPIRE].

[43] F. Rahaman, M. Kalam and S. Chakraborty, *Thin shell wormholes in higher dimensional Einstein-Maxwell theory*, *Gen. Rel. Grav.* **38** (2006) 1687 [gr-qc/0607061] [INSPIRE].

[44] C. Bejarano, E.F. Eiroa and C. Simeone, *Thin-shell wormholes associated with global cosmic strings*, *Phys. Rev.* **D 75** (2007) 027501 [gr-qc/0610123] [INSPIRE].

[45] F. Rahaman, M. Kalam and S. Chakraborti, *Thin shell wormhole in heterotic string theory*, *Int. J. Mod. Phys.* **D 16** (2007) 1669 [gr-qc/0611134] [INSPIRE].

[46] E.F. Eiroa and C. Simeone, *Stability of Chaplygin gas thin-shell wormholes*, *Phys. Rev.* **D 76** (2007) 024021 [arXiv:0704.1136] [INSPIRE].

[47] F. Rahaman, M. Kalam, K.A. Rahman and S. Chakraborti, *A theoretical construction of thin shell wormhole from tidal charged black hole*, *Gen. Rel. Grav.* **39** (2007) 945 [gr-qc/0703143] [INSPIRE].

[48] M.G. Richarte and C. Simeone, *Traversable wormholes in a string cloud*, *Int. J. Mod. Phys.* **D 17** (2008) 1179 [arXiv:0711.2297] [INSPIRE].

[49] E. Poisson and M. Visser, *Thin shell wormholes: linearization stability*, *Phys. Rev.* **D 52** (1995) 7318 [gr-qc/9506083] [INSPIRE].

[50] F.S.N. Lobo and P. Crawford, *Linearized stability analysis of thin shell wormholes with a cosmological constant*, *Class. Quant. Grav.* **21** (2004) 391 [gr-qc/0311002] [INSPIRE].

[51] D. Horvat, S. Ilijic and A. Marunovic, *Radial stability analysis of the continuous pressure gravastar*, *Class. Quant. Grav.* **28** (2011) 195008 [arXiv:1104.3537] [INSPIRE].

[52] S.S. Yazadjiev and D.D. Doneva, *Possible dark energy imprints in gravitational wave spectrum of mixed neutron-dark-energy stars*, *JCAP* **03** (2012) 037 [arXiv:1112.4375] [INSPIRE].

JHEP12(2013)065

[53] E. Witten, *Bound states of strings and p-branes*, *Nucl. Phys.* **B 460** (1996) 335 [hep-th/9510135] [INSPIRE].

[54] N. Seiberg and E. Witten, *String theory and noncommutative geometry*, *JHEP* **09** (1999) 032 [hep-th/9908142] [INSPIRE].

[55] A. Smailagic and E. Spallucci, *Feynman path integral on the noncommutative plane*, *J. Phys.* **A 36** (2003) L467 [hep-th/0307217] [INSPIRE].

[56] P. Nicolini, A. Smailagic and E. Spallucci, *Noncommutative geometry inspired Schwarzschild black hole*, *Phys. Lett.* **B 632** (2006) 547 [gr-qc/0510112] [INSPIRE].

[57] E. Di Grezia, G. Esposito and G. Miele, *Black hole evaporation in a spherically symmetric non-commutative space-time*, *J. Phys.* **A 41** (2008) 164063 [arXiv:0707.3318] [INSPIRE].

[58] R. Casadio and P. Nicolini, *The decay-time of non-commutative micro-black holes*, *JHEP* **11** (2008) 072 [arXiv:0809.2471] [INSPIRE].

[59] P. Nicolini, *Noncommutative black holes, the final appeal to quantum gravity: a review*, *Int. J. Mod. Phys.* **A 24** (2009) 1229 [arXiv:0807.1939] [INSPIRE].

[60] E. Spallucci, A. Smailagic and P. Nicolini, *Non-commutative geometry inspired higher-dimensional charged black holes*, *Phys. Lett.* **B 670** (2009) 449 [arXiv:0801.3519] [INSPIRE].

[61] S. Ansoldi, P. Nicolini, A. Smailagic and E. Spallucci, *Noncommutative geometry inspired charged black holes*, *Phys. Lett.* **B 645** (2007) 261 [gr-qc/0612035] [INSPIRE].

[62] P. Nicolini, *A model of radiating black hole in noncommutative geometry*, *J. Phys.* **A 38** (2005) L631 [hep-th/0507266] [INSPIRE].

[63] R. Garattini and F.S.N. Lobo, *Self sustained phantom wormholes in semi-classical gravity*, *Class. Quant. Grav.* **24** (2007) 2401 [gr-qc/0701020] [INSPIRE].

[64] R. Garattini and F.S.N. Lobo, *Self-sustained wormholes in modified dispersion relations*, *Phys. Rev.* **D 85** (2012) 024043 [arXiv:1111.5729] [INSPIRE].

[65] R. Garattini and F.S.N. Lobo, *Self-sustained traversable wormholes in noncommutative geometry*, *Phys. Lett.* **B 671** (2009) 146 [arXiv:0811.0919] [INSPIRE].

[66] K. Lanczos, *Flächenhafte Verteiliung der Materie in der Einsteinschen Gravitationstheorie*, *Ann. Phys. (Leipzig)* **74** (1924) 518.

[67] G. Darmois, *Les équations de la gravitation einsteinienne*, in *Mémorial des sciences mathématiques*, Fascicule XXV, Gauthier-Villars, Paris France (1927).

[68] W. Israel, *Singular hypersurfaces and thin shells in general relativity*, *Nuovo Cim.* **B 44** (1966) 1 [*Erratum ibid.* **B 48** (1967) 463] [INSPIRE].

[69] A. Papapetrou and A. Hamoui, *Simple material layers in general relativity*, *Ann. Inst. Henri Poincaré* **9** (1968) 179.

[70] N.M. Garcia, F.S.N. Lobo and M. Visser, *Generic spherically symmetric dynamic thin-shell traversable wormholes in standard general relativity*, *Phys. Rev.* **D 86** (2012) 044026 [arXiv:1112.2057] [INSPIRE].

[71] P. Martin Moruno, N. Montelongo Garcia, F.S.N. Lobo and M. Visser, *Generic thin-shell gravastars*, *JCAP* **03** (2012) 034 [arXiv:1112.5253] [INSPIRE].

[72] K.A. Bronnikov, R.A. Konoplya and A. Zhidenko, *Instabilities of wormholes and regular black holes supported by a phantom scalar field*, *Phys. Rev.* **D 86** (2012) 024028 [arXiv:1205.2224] [INSPIRE].

JHEP12(2013)065